Quantum Interference Effects in the Ultraviolet Photolysis of Ar−HCl Following Total Fragmentation into H + Ar + Cl

J. C. Juanes-Marcos and A. García-Vela*

Instituto de Matemáticas y Física Fundamental, CSIC, Serrano 123, 28006 Madrid, Spain

Received: January 11, 2002; In Final Form: March 27, 2002

The total fragmentation pathway of Ar−HCl upon ultraviolet photoexcitation, Ar−HCl + $h\nu \rightarrow$ H + Ar + Cl, is studied using a wave packet treatment. Kinetic-energy distributions of the hydrogen fragment are calculated for different excitation energies of the cluster. The distributions display a structure of peaks that can be assigned to successive collisions of hydrogen with Ar and Cl before dissociating. Up to four peaks with decreasing intensity as the kinetic energy decreases are found in the distributions in the range of kinetic energies investigated. The two most intense peaks appearing at high kinetic energies are assigned to the first H/Ar collision, the main peak associated with weak collisions, and the other one associated with harder collisions. Two additional peaks at lower kinetic energies are assigned to subsequent hydrogen collisions, i.e., a second collision with Cl and a third one with Ar again, respectively. The structure of the H fragment kinetic-energy distributions is the signature of interference between the fragment states populated through the successive hydrogen collisions. Classical H fragment distributions are found to be unstructured, which provides a confirmation that the above structure is produced by quantum interference effects. At least part of the structure is intense enough as to be observed experimentally. The mechanism of total fragmentation of the cluster is analyzed and discussed.

I. Introduction

The ultraviolet (UV) photolysis of hydrogen-bonded clusters has attracted growing interest in the past decade. These systems are composed of a chromophore that contains (at least) one hydrogen atom (e.g., HX or H_2Y, X = halogen, Y = O, S), weakly bound to one or more rare gas atoms or molecular species. By UV photoexcitation a large amount of energy is deposited in the chromophore, causing fast ejection of a hot H fragment. Upon the H atom recoil, the cluster can follow different fragmentation pathways. Direct dissociation of the hydrogen may leave behind open-shell radical complexes[1−4] with a distribution of ro-vibrational excitations, which allows one to probe the open-shell interactions involved. More extensive fragmentation can occur in collisional events where the recoiling hydrogen collides with the species weakly bound to the chromophore. The restricted range of initial relative geometries of the weakly bound species within the cluster determines, to a large extent, the branching ratio between the probability of the different fragmentation pathways.

Experimental work on UV photolysis of H-bonded precursors has focused mainly on small clusters of the type Ar−HBr,[1,5] Ar−HI,[1] $(HI)_2$,[2] $(HCl)_2$,[3,6] Ar_n-H_2S ($n \leq 2$),[4] and Ar−H_2O.[7,8] Photolysis of larger clusters such as $(HI)_n$[9] and $(HBr)_n$[10] with $n > 2$ was also investigated experimentally. The UV photodissociation of a variety of clusters has also been explored from the theoretical point of view.[5,11−14] In particular, the UV photolysis of Ar−HCl has been extensively studied theoretically using different methods,[15−24] among them exact quantum mechanical, energy-resolved calculations.[22−24]

Photolysis of Ar−HCl occurs via two possible fragmentation pathways. These two pathways are

$$\text{Ar−HCl} + h\nu \rightarrow \text{H} + \text{Ar−Cl} \quad (1)$$

$$\text{Ar−HCl} + h\nu \rightarrow \text{H} + \text{Ar} + \text{Cl} \quad (2)$$

The partial fragmentation (PF) pathway (1) implies a direct dissociation mechanism of the H fragment. The total fragmentation (TF) pathway (2) involves (at least) one collision of the recoiling hydrogen with Ar, and subsequent energy transfer to the Ar−Cl bond. Energy-resolved studies[23,24] have shown that the TF pathway is clearly dominant at most of the excitation energies in the region covered by the Ar−HCl absorption spectrum. The PF pathway dominates only at very low excitation energies.

A global interpretation of the UV photolysis of Ar−HCl was recently proposed.[24] This interpretation involves a mechanism of interference between product fragment states populated by the fragmentation pathways (1) and (2), which occur simultaneously at the different excitation energies of the parent cluster. Interference between fragment states would be induced by the H/Ar collision. In ref 24 the effects of the interference mechanism on the product distributions of the PF pathway were analyzed. The main goal of the present work is to explore the possible manifestations of interference in the TF pathway of Ar−HCl. To this purpose, energy-resolved distributions associated with the H fragment produced by total fragmentation are calculated and analyzed for different excitation energies of Ar−HCl.

The outline of the paper is the following. Details of the methodology applied are described in section II. In section III

* Corresponding author. E-mail: garciavela@imaff.cfmac.csic.es.

10.1021/jp020081g CCC: $22.00
Published on Web 05/08/2002

the calculated H fragment distributions are reported and discussed. Some concluding remarks are given in section IV.

II. Theoretical Treatment

Ultraviolet excitation of Ar−HCl is achieved by promoting vertically its ground ro-vibrational state from the ground electronic state $X^1\Sigma^+$ of the H−Cl chromophore to the excited electronic state $A^1\Pi$. Then, the cluster photolysis is simulated by an exact wave packet propagation (assuming $J = 0$) in the upper potential surface. The wave packet is represented in Jacobian coordinates (r, R, θ), where r is the HCl distance, R is the separation between the Ar atom and the HCl center-of-mass, and θ is the angle between the vectors **r** and **R**. The angle $\theta = 0°$ corresponds with the collinear configuration of the cluster with the hydrogen between Ar and Cl (the equilibrium geometry). Details on the ground and excited potential surfaces used[19,20] and on the wave packet propagation[20] have been given in previous works. At the end of the propagation ($t_f = 80$ fs), the asymptotic wave packet $\Phi(r,R,\theta,t_f)$ is projected out onto the asymptotic states describing fragmentation into H + Ar + Cl, for several excitation energies of Ar−HCl.

Energy-resolved studies on the Ar−HCl TF pathway were first reported in ref 22, where kinetic-energy distributions of the hydrogen fragment were calculated. However, such distributions were restricted to H atoms extensively cooled after one or more collisions with Ar and Cl. The reason of this restriction was the following. The three-fragment asymptotic states were represented in the same Jacobian coordinates, (r, R, θ), as the asymptotic wave packet $\Phi(r,R,\theta,t_f)$. The advantage is that in this case the wave packet projection is computationally simple and relatively inexpensive. The disadvantage is that in the (r, R, θ) representation the PF asymptotic states are not well defined, and they are nonorthogonal with the TF ones, as discussed in ref 22. As a consequence, there are regions of the wave packet where the PF and TF asymptotic states defined in the (r, R, θ) representation are mixed and cannot be separated by projection. To overcome this difficulty, an approximate partition of the asymptotic wave packet was established in ref 22, to ensure that the part of the wave packet projected onto TF asymptotic states was free of PF components. The part of wave packet containing PF components and not included in the projection quadratures, also contained TF components associated with hot (high-kinetic-energy) H atoms. As a result, the intensity corresponding to the high-kinetic-energy region of the H fragment distributions of ref 22 is missing.

In the present work we have followed a more rigorous treatment, which allows one to obtain the distribution in the whole range of kinetic energies accessible to the H fragment. This treatment involves the representation of both the TF and the PF asymptotic states in another Jacobian coordinates, (R', r', θ'), where the two sets of states are well-defined and are orthogonal to each other. The (R', r', θ') coordinates (used in ref 24 to represent the PF states) are such that R' is the distance between H and the Ar−Cl center-of-mass, r' is the Ar−Cl separation, and θ' is the angle between the vectors **R′** and **r′**. The angle $\theta' = 0°$ corresponds to the collinear configuration of Ar−HCl with the hydrogen between Ar and Cl, and the **R′** vector pointing toward the Ar atom.

The rigorous definition of orthogonal TF and PF states by using the (R', r', θ') representation implies a computationally far more expensive calculation of the H fragment distributions than in ref 22. Now, the TF states have to be transformed (through a Jacobian transformation) from the (R', r', θ') representation to the (r, R, θ) one where the wave packet is represented, to carry out the projection quadratures. This transformation is costly since a large and dense grid is needed to accurately describe the double-continuum, highly oscillating TF states. In addition, due to the double-continuum character of the TF pathway, a large number of TF states has to be considered in the projection calculation for each excitation energy of the cluster.

For an ideally asymptotic wave packet the H + Ar + Cl fragment states for a total energy E can be represented as

$$\chi^{(E)}_{\epsilon_{kR'},\epsilon_{kr'},j}(R',r',\theta',t) = (\mu_{R'}/2\pi k_R\hbar^2\mu_{r'}/2\pi k_{r'}\hbar^2)^{1/2} e^{ik_{R'}R'} e^{ik_{r'}r'} P_j(\cos\theta') e^{-iEt/\hbar} \quad (3)$$

where $\mu_{R'}$ and $\mu_{r'}$ are the reduced masses associated with R' and r', respectively, $\epsilon_{k_{R'}}$ and $\epsilon_{k_{r'}}$ are the kinetic energies associated with the relative translational motion between the fragments along the coordinates R' and r', respectively [$k_{R'} = (2\mu_{R'}\epsilon_{k_{R'}})^{1/2}/\hbar$, $k_{r'} = (2\mu_{r'}\epsilon_{k_{r'}})^{1/2}/\hbar$], and $P_j(\cos\theta')$ is a normalized Legendre polynomial. In the asymptotic limit the total energy can be expressed as

$$E = \epsilon_{k_{R'}} + \epsilon_{k_{r'}} \quad (4)$$

In our case, at the end of the propagation the wave packet is asymptotic regarding the separation between H and the Ar−Cl center-of-mass, but it is not completely asymptotic in the Ar−Cl separation. As we shall see below, the reason is that most of the wave packet intensity corresponds to fragmentation into a very hot H fragment and rather cold Ar and Cl fragments. The heavy, slow-moving Ar and Cl fragments take a long time (much longer than our propagation time) to separate and reach the asymptotic region. A wave packet propagation long enough to ensure that the wave packet is completely asymptotic in the Ar−Cl separation would be extremely costly. Actually, we believe that such a long propagation is unncessary in order to calculate asymptotic H fragment distributions, as we shall discuss below.

Since most of our "asymptotic" wave packet is still in the interaction region of the Ar−Cl separation, a more appropriate definition than that of eq 3 of the TF asymptotic states onto which the wave packet is to be projected out is

$$\xi^{(E)}_{\epsilon_{kR'},\epsilon_{kr'},j}(R',r',\theta',t) = (\mu_{R'}/2\pi k_R\hbar^2)^{1/2} e^{ik_{R'}R'} \varphi^{(j)}_{\epsilon_{kr'}}(r') P_j(\cos\theta') e^{-iEt/\hbar} \quad (5)$$

where $\varphi^{(j)}_{\epsilon_{kr'}}(r')$ is an eigenstate of the continuum spectrum of the Ar−Cl stretch mode for a given j state, with energy $\varphi_{\epsilon_{kr'}}$, obtained as a numerical solution of

$$\left[-\frac{\hbar^2}{2\mu_{r'}}\frac{\partial^2}{\partial r'^2} + \frac{j(j+1)\hbar^2}{2\mu_{r'}(r')^2} + V_{\mathrm{Ar-Cl}}(r')\right]\varphi^{(j)}_{\epsilon_{kr'}}(r') = \epsilon_{k_{r'}}\varphi^{(j)}_{\epsilon_{kr'}}(r') \quad (6)$$

Solution of eq 6 involves the use of a large domain in the r' coordinate, 1 au $\leq r' \leq$ 550 au, to ensure the correct asymptotic behavior of $\varphi^{(j)}_{\epsilon_{kr'}}(r')$. The functions $\varphi^{(j)}_{\epsilon_{kr'}}(r')$ have nonzero amplitude in the interaction region of the r' coordinate.

We note that the basis of TF asymptotic states of eq 5 is as valid as the basis of asymptotic states of eq 3 in order to represent the TF components of our wave packet. The only difference between the two types of asymptotic states is the region of phase space that they cover. The states of eq 3 are eigenstates of the asymptotic Hamiltonian when both $R' \rightarrow \infty$

and $r' \rightarrow \infty$. The states of eq 5 are eigenstates of the asymptotic Hamiltonian that includes the whole domain in r' and the asymptotic region of R' ($R' \rightarrow \infty$). This latter basis of asymptotic states is more adapted to represent the situation of our asymptotic wave packet.

It remains to be shown that though our wave packet is not fully asymptotic in the Ar−Cl internuclear separation, the H fragment distributions projected out of it are actually asymptotic. This is a consequence of conservation of total energy and angular momentum of the triatomic system, and the fact that the H atom is already in the asymptotic region. Indeed, once the H atom leaves the interaction region, there is no possibility of interaction, and therefore of energy and angular momentum exchange, between H and the Ar + Cl subsystem. Thus, to conserve total energy and angular momentum of the three-fragment system, population generated in a state $\varphi^{(j)}_{\epsilon_{kR'}}(r')P_j(\cos\theta')$ of the Ar + Cl subsystem when H reaches the asymptotic region ($R' \rightarrow \infty$) must remain in that state for any further time. Interference and population transfer between different $\varphi^{(j)}_{\epsilon_{kR'}}(r')P_j(\cos\theta')$ states of the wave packet would imply exchange of energy and/or angular momentum between the H and Ar + Cl subsystems, not possible due to the absence of interaction between them. Therefore, to extract asymptotic H fragment distributions out of the wave packet, it must be asymptotic in the H dissociation coordinate (which is the case of our final wave packet), but not necessarily so in the Ar−Cl coordinate.

By means of a Jacobian transformation the asymptotic state $\xi^{(E)}_{\epsilon_{kR'},\epsilon_{kr'},j}(R',r',\theta',t)$ can be expressed as a state $\eta^{(E)}_{\epsilon_{kR'},\epsilon_{kr'},j}(r,R,\theta,t)$ in the (r, R, θ) coordinates.[23a] Now the wave packet $\Phi(r,R,\theta,t_f)$ is projected out onto the states $\eta^{(E)}_{\epsilon_{kR'},\epsilon_{kr'},j}(r,R,\theta,t_f)$,

$$c_j(\epsilon_{k_{R'}},E) = \langle \eta^{(E)}_{\epsilon_{kR'},\epsilon_{kr'},j}(r,R,\theta,t_f)|\Phi(r,R,\theta,t_f)\rangle \qquad (7)$$

providing the amplitudes $c_j(\epsilon_{kR'},E)$ of Ar−HCl photofragmentation into H + Ar + Cl products in the different asymptotic states for an energy E. Converged coefficients $c_j(\epsilon_{kR'},E)$ are obtained by interpolating the final wave packet following a procedure that was already described in ref 23b. A small portion of the wave packet that is still not asymptotic in the hydrogen dissociation coordinate at $t = t_f$ (7%, corresponding to $r < 19.9$ au) has been removed[23a] from the projection quadrature of eq 7. Note that the index $\epsilon_{k_{r'}}$ has been dropped in $c_j(\epsilon_{kR'},E)$, since it is automatically determined by energy conservation (eq 4) once E and $\epsilon_{k_{R'}}$ are specified.

The kinetic-energy distribution (KED) in the R' coordinate for a given energy E can be calculated as

$$P(\epsilon_{k_{R'}},E) = \sum_j |c_j(\epsilon_{k_{R'}},E)|^2 \qquad (8)$$

Taking into account that the kinetic energy of the H fragment is $\epsilon^H_k = (m_{Ar} + m_{Cl}/m_H + m_{Ar} + m_{Cl})\epsilon_{kR'}$, the H fragment KED, $P(\epsilon^H_k,E)$, can be easily obtained from $P(\epsilon_{kR'},E)$ by changing from the $\epsilon_{kR'}$ variable to the ϵ^H_k. The $P(\epsilon^H_k,E)$ distribution corresponds to the hydrogen time-of-flight (TOF) spectrum measured with a detector scanning all possible final scattering angles of the fragment, after a monochromatic excitation to an energy E of the Ar−HCl cluster.

The $P(\epsilon_{kR'},E)$ distributions associated with four different excitation energies of Ar−HCl in the range of the absorption spectrum have been calculated. For each distribution typically 70 points in the $\epsilon_{kR'}$ energy domain were calculated in a range of 0.85 eV. For each energy $\epsilon_{kR'}$ several j states had to be included in eq 8. Depending on the value of E and $\epsilon_{kR'}$, the number of j states ranged from 70 for the highest $\epsilon_{kR'}$ energies corresponding to the lowest E energy to 220 for the lowest $\epsilon_{kR'}$ energies corresponding to the highest E energy. Convergence in the number of j states was checked for the different $\epsilon_{kR'}$ energies. The total number of degenerate states $\eta^{(E)}_{\epsilon_{kR'},\epsilon_{kr'},j}(r,R,\theta,t_f)$ included in each distribution ranged from about 9800 for the lowest E up to about 12 400 for the highest E. A further test was carried out by checking that $P_{total}(E) = P_{TF}(E) + P_{PF}(E)$ (taking into account the 7% of wave packet removed from the projection quadratures), where

$$P_{TF}(E) = \int d\epsilon_{k_{R'}} P(\epsilon_{k_{R'}},E) \qquad (9)$$

and $P_{total}(E)$ and $P_{PF}(E)$ were calculated in ref 23 ($P_{PF}(E)$ was denoted as $P_{Ar-Cl}(E)$ in that work).

Classical kinetic-energy distributions of the H fragment have also been calculated in order to compare with the quantum mechanical ones. Initial conditions corresponding to different excitation energies of Ar−HCl were sampled from the quantum distribution associated with the initial wave packet, following a method recently proposed[25] and also applied in ref 24. For all the excitation energies the energy dispersion of the initial conditions was $\Delta E = \pm 10$ cm^{-1}.

III. Results and Discussion

A. Kinetic-Energy Distributions of the Hydrogen Fragment. The quantum mechanical H fragment KED has been calculated for four different excitation energies of Ar−HCl, and the results are shown in Figures1−4. The dashed line displayed in each figure marks the limit to the right of which is the energy region where the intensity corresponding to hydrogen fragments produced by the PF pathway appears. We note, however, that the distributions of Figures 1−4 correspond only to H fragments produced by the TF pathway.

All the distributions present the same pattern, consisting of a main peak at high kinetic energies, a secondary and broad peak at somewhat lower kinetic energies, and a tail extending toward the region of low ϵ^H_k. As shown by the insets of the figures, the tails of the distributions also display a structure of peaks. Our interpretation is that the structure found in the H fragment KED is caused by interference between TF states produced by one or more collisions of H with Ar and Cl. In ref 20 the time evolution of the wave packet was analyzed (see Figure 2 of that work). Upon the first collision with the Ar obstacle, the wave packet components interfere and break into three pieces. Two of the pieces continue traveling toward the asymptotic region, one of them centered around $\theta = 50°$ (the main piece) and the other, smaller one centered around $\theta = 20°$. A third portion of wave packet remains between Ar and Cl, undergoing further collisions with Cl and Ar and subsequently leaving the interaction region. On the basis of the similarity of intensities, the main and the secondary peak of each H fragment KED can be assigned to the wave packet pieces centered at $\theta = 50°$ and $\theta = 20°$, respectively. The tails of the distributions at lower energies ϵ^H_k would correspond to (part of) the third piece of wave packet, which undergoes a more extensive cooling of the hydrogen.

Classical calculations of the H fragment KED were carried out for three excitation energies, $E = 1.82$, 2.87, and 3.92 eV, for which 7519, 42 867, and 22 674 trajectories were integrated, respectively. The classical distributions are shown in Figure 5 along with the corresponding quantum mechanical ones. Good qualitative agreement between the quantum and classical distributions is found for the three energies. Interestingly,

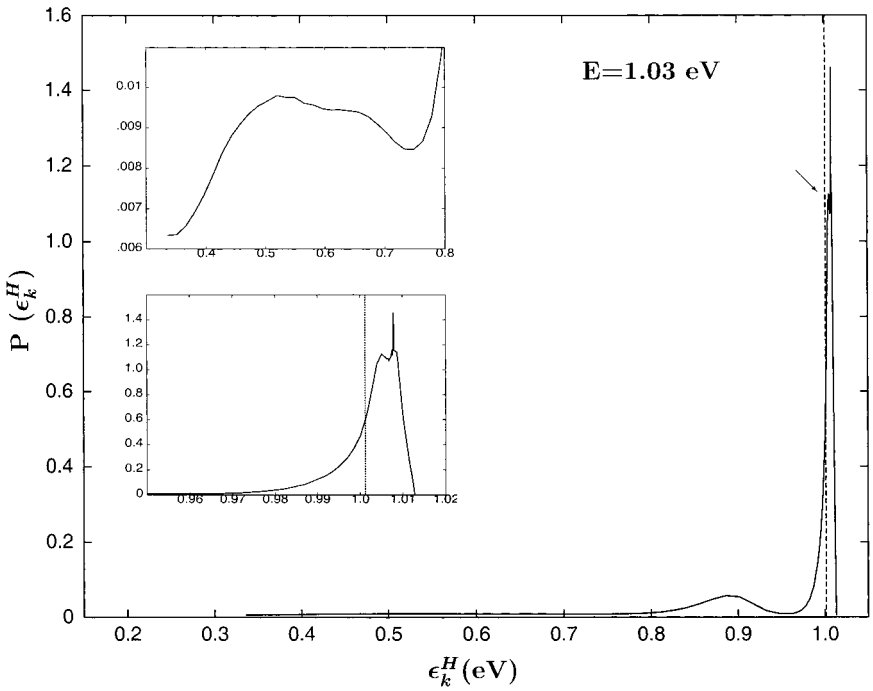

Figure 1. Kinetic-energy distribution of the H fragment for an excitation energy of Ar−HCl $E = 1.03$ eV. The limit $E = 0$ corresponds to three separated atoms. The insets show expanded views of the tail at low kinetic energies and the main peak of the distribution. See the text for details.

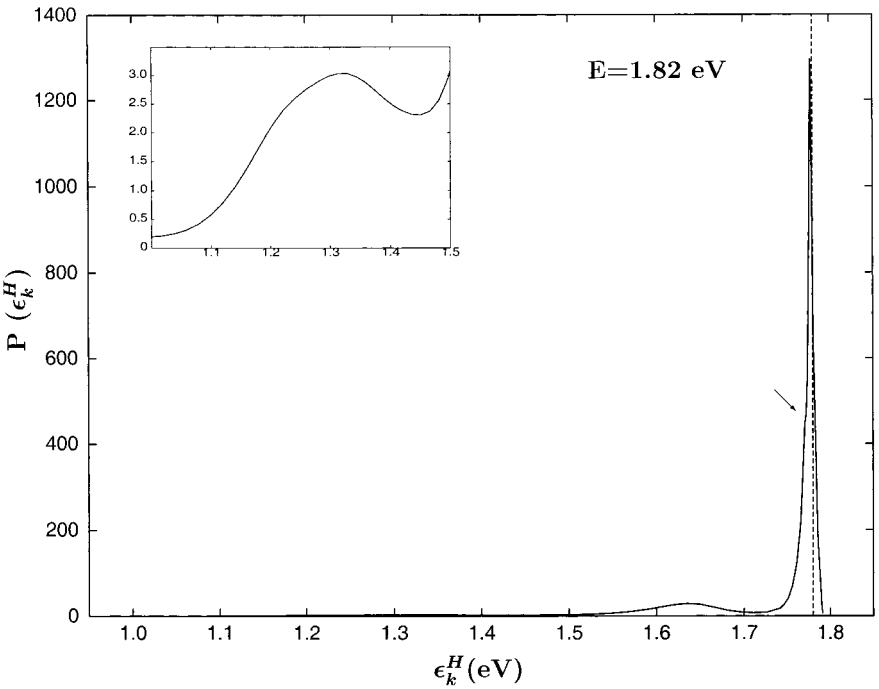

Figure 2. Same as Figure 1 for $E = 1.82$ eV. The inset shows an expanded view of the tail of the distribution at low kinetic energies. See the text for details.

however, the classical distributions are unstructured, consisting of a main peak and a tail with monotonically decreasing intensity as ϵ_k^H decreases. The classical result provides an additional confirmation of our interpretation that the structure in the quantum H KED is produced by an interference effect.

In the remaining of section III.A we shall discuss the quantum H fragment distributions of Figures 1−4. Most of the intensity of each hydrogen KED concentrates in the main peak of the distribution, which appears at kinetic energies close to the total energy E excited. It indicates that most of the TF events produce a very hot H fragment, which carries almost all the available energy, and very cold Ar and Cl fragments. Such events involve a nearly direct hydrogen dissociation through rather weak, side collisions between H and Ar, where energy transfer is not very effective. This is consistent with assigning this main peak to the wave packet piece appearing at larger angles, as discussed above. The secondary, broader peak of the KED involves more effective energy transfer, ranging from 0.05−0.23 eV for $E =$ 1.03 eV to 0.10−0.38 eV for $E = 3.92$ eV. This peak is produced by somewhat harder H/Ar collisions, at smaller initial orientations of hydrogen with respect to Ar.

We note that part of the main peak of the distributions overlaps with the energy region of the H + Ar−Cl fragments where Ar−Cl is produced in quasibound states[23,24] (with energy

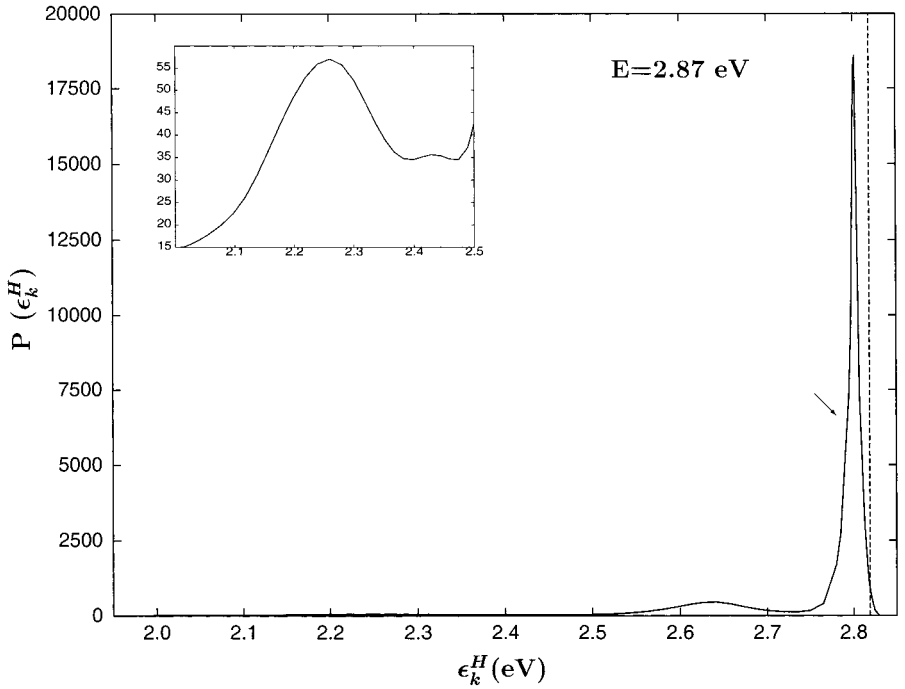

Figure 3. Same as Figure 2 for $E = 2.87$ eV.

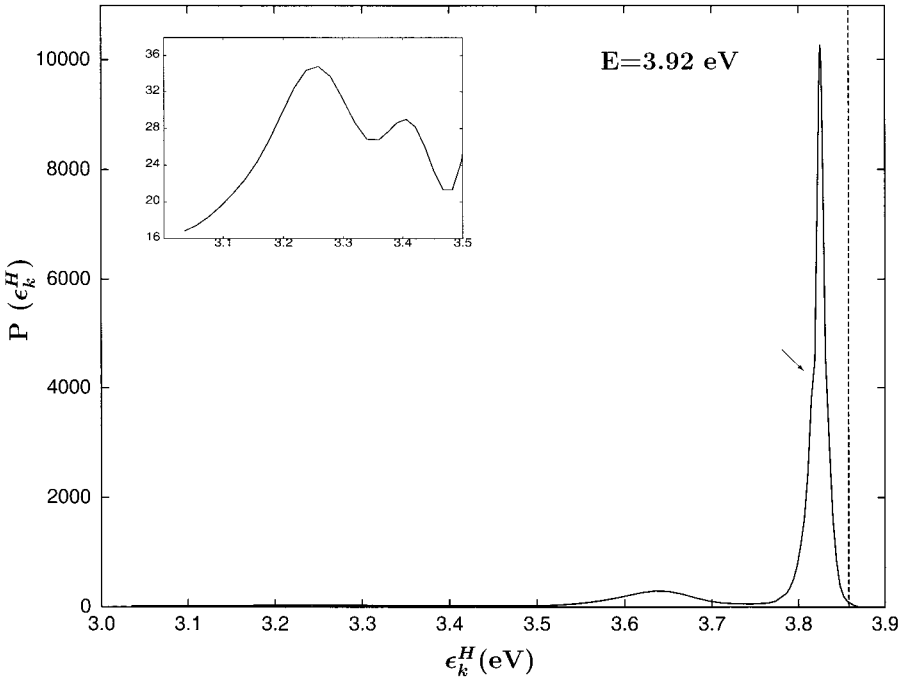

Figure 4. Same as Figure 2 for $E = 3.92$ eV.

above the dissociation limit of the Ar−Cl potential). In particular, at very low excitation energies (like $E = 1.03$ eV) most of the main peak falls into this energy region. This degeneracy or near degeneracy of quasibound PF states with some TF states may favor interference between them upon the first H/Ar collision. The overlapping between the populated regions of TF states of the main peak and quasibound PF states decreases with increasing E.

It is interesting to note the structure appearing in the main peak of the KED for $E = 1.03$ eV (indicated by an arrow). An expanded view of this peak is shown in one of the insets of Figure 1. Similar, although weaker "shoulders" also appear in the other three hydrogen distributions (indicated by the arrows). These weak features of the different distributions can have two possible origins. One of them is interference, upon the H/Ar collision, between TF states associated with high kinetic energies of hydrogen. The other possibility is the above-mentioned interference between PF and TF states, of the type described in ref 24. Upon relatively weak H/Ar collisions, population initially in PF states (with Ar−Cl either in bound or quasibound states) is promoted to TF states associated with a low kinetic energy of the Ar and Cl fragments (and a high ϵ_k^{H}). This would cause local increases in the intensity of the main peak of the H fragment KED, consistent with the weak features found. Unfortunately, with the information available at present it is not possible to discriminate between the two possible origins.

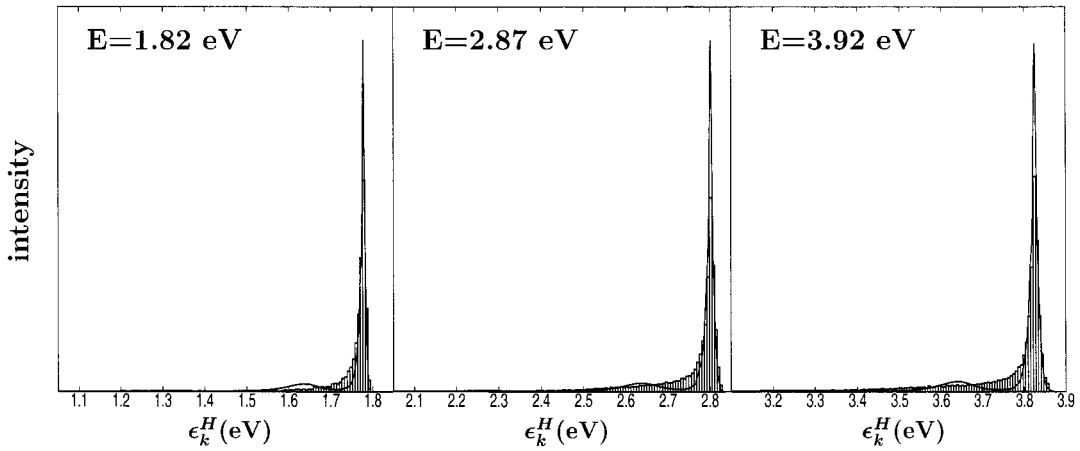

Figure 5. Classical H fragment kinetic-energy distributions (histograms) for three excitation energies of the cluster. The corresponding quantum mechanical distributions (solid lines) are also shown for comparison. The quantum and classical distributions have been normalized to unity.

The insets of Figures 1−4 show an expanded view of the low-kinetic-energy tails of the H fragment distributions. The extensive cooling undergone by the hydrogen fragments associated with the intensity of these tails involves further collisions with Cl and Ar. Actually, the tails of the distributions display a weak structure of two overlapping peaks. The only exception is the KED for $E = 1.82$ eV, where only one broad peak appears in the tail, probably as a result of the superposition of the two overlapping peaks. In the cases of $E = 1.03$ eV and $E = 2.87$ eV the structure of two peaks is very diffuse, while for $E = 3.92$ eV the two peaks are clearly distinct.

The two peaks of the tails, as ϵ_k^{H} decreases, are produced by interference between TF states caused by a second and third collision of hydrogen with Cl and Ar, respectively. The peak at higher energies ϵ_k^{H}, corresponding to the H/Cl collision has a lower intensity than that corresponding to the second H/Ar collision (at lower energies ϵ_k^{H}). The reason is that only part of the wave packet components trapped in the interaction region dissociate after the H/Cl collision, giving rise to the smaller peak of the tail. Most of these trapped components still undergo a subsequent collision with Ar, after which they dissociate, producing the more intense peak at lower kinetic energies in the tail. We shall return to this point in section III.B. Leaving aside the main peak of each KED, which corresponds to weak H/Ar collisions, the three remaining peaks (the secondary one and the two peaks of the tail) would be associated with relatively hard collisions of hydrogen with Ar, Cl, and Ar again, respectively. For a given excitation energy, the separation between these three peaks decreases as ϵ_k^{H} decreases, due to the fact that as the hydrogen is cooled by the successive collisions, it transfers less energy per collision. The broad spreading in energy of these three bumps reflects the wide range of orientations along which the H/Ar and H/Cl collisions occur. Such different orientations lead to quite different amounts of energy transferred in the collisional event.

As the range of low energies ϵ_k^{H} is extended beyond that of the present distributions, additional peaks with decreasing intensity are expected, corresponding to further hydrogen collisions, as shown in ref 22. However, a correct calculation of the hydrogen KED at kinetic energies lower than the present ones would imply inclusion of the portion of the hydrogen wave packet that is still not asymptotic in the r coordinate at $t = t_{\mathrm{f}}$. When these wave packet components become asymptotic, they will contribute to the region of very low ϵ_k^{H} of the KED.

In the following we shall analyze the effect of increasing excitation energy on the H KED. As E increases, the main peak of the distributions appears at lower kinetic energies. This decrease of the maximum energy available for the H fragment is due to the combination of two factors. On one hand, the energy transferred in the first H/Ar collision increases, and on the other hand, the recoil energy available for the center-of-mass of the Ar + Cl subsystem increases as well. The secondary peak shifts also toward lower ϵ_k^{H} and becomes increasingly separated from the main peak as the excitation energy increases. Also the peaks of the distribution tails increase the separation between them, and from the secondary peak. This is a consequence of the larger amount of energy transferred in each collision with increasing E. A gradual broadening of both the main and the secondary peak takes place as E increases. It is found that the ratio between the areas under the secondary and the main peak decreases as E becomes higher. The implication is that, concerning the first H/Ar collision, the weight of the weak collisions becomes increasingly important as compared with that of the stronger ones.

The similarity of the main structure found in the hydrogen distributions at different energies E supports our interpretation that these patterns are produced by interference basically only between TF states. It was found in refs 23 and 24 that in the range of excitation energies investigated the probability of the PF pathway, and therefore the population of PF states, changes substantially. Thus, if the main structure of the H fragment KED was caused to a relevant extent by interference between PF and TF states, we would expect larger changes in this structure as E increases. More specifically, if there was a relevant effect of interference between PF and TF states on the secondary peak and on the two peaks of the KED tail, one should expect superimposed on those peaks a finer structure of local increases of intensity, similar to those displayed by the main peaks of the distributions. This finer structure is absent even in the case of $E = 1.03$ eV, where the population of PF states and therefore the probability of interference between PF and TF states is higher. Such a result seems to indicate that the effect of PF/TF interference on the H KED at kinetic energies lower than those of the main peak is very small, or even nonexistent. In addition, the similarity of the structure displayed by the different distributions makes unlikely that such a structure is the reflection of the shape of the cluster wave function excited at each energy (following the reflection principle). The excitation energies investigated are different enough as to make very unlikely that the cluster wave functions associated with them have a similar shape.

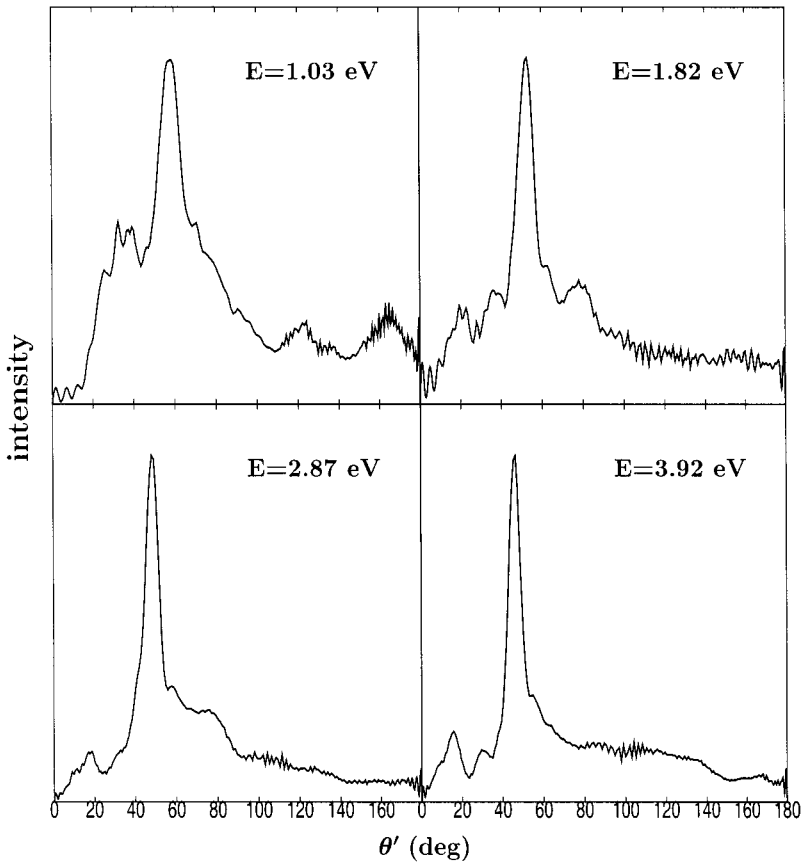

Figure 6. Angular distributions of the hydrogen fragment for the four excitation energies of Ar−HCl studied. See the text for details.

The structure manifested in the hydrogen KED is related to interference between broad and overlapping excited-state resonances associated with chattering of H between Ar and Cl. The existence and observable manifestations of such resonances in Ar−HCl have been investigated by several groups.[15,16,18,21,22] The structure present in the low-kinetic-energy tail of the KED was already found in the earlier energy-resolved calculations of ref 22. The main novelty of the present work is that it extends the calculation of the H fragment KED to the region of higher kinetic energies, and additional structure consisting of the secondary and the main peaks appears. While the intensity of the KED tails is rather low to be detected, the intensity of the secondary peak seems to be high enough for all excitation energies as to be experimentally observed. Therefore, the structure formed by the main and the secondary peaks would be the observable signature of interference between broad resonances associated with short trapping of hydrogen involving only one collision with Ar. The implication is that, for other systems where further hydrogen collisions are likely enough, the intensity of the structure at lower H kinetic energies should also be high enough as to be detected.

B. Angular Distributions of the H Fragment. The angular distributions of the hydrogen fragment provide additional information on the Ar−HCl photolysis through the TF pathway. Quantum mechanical angular distributions associated with the four excitation energies studied in this work are shown in Figure 6. The sin θ' factor of the volume element in the Jacobian coordinates (R', r', θ') has been included in the distributions.

The H fragment angular distributions for the different excitation energies show a qualitatively similar shape. This is consistent with the result that the kinetic-energy distributions of Figures 1−4 are also qualitatively similar. All the angular distributions spread over the whole angular range and display a structure of peaks, one of them particularly intense around $\theta' = 50°$. The large spreading of the distributions is consistent with the wide range of orientations along which hydrogen collides with the heavier atoms. Actually, the angular distributions of Figure 6 closely resemble the shape of the angular distribution associated with the whole wave packet[26] (see Figure 5b of ref 20). The similarity of the angular distributions of Figure 6 indicates that the TF pathway proceeds in a similar way in the range of excitation energies covered by the absorption spectrum of Ar−HCl. As E increases, the main effects are that the intensity at very small and large angles decreases, and the angular distributions become less structured. The structure of peaks displayed by the angular distributions of Figure 6 is a manifestation of quantum interference between the TF states populated upon the different hydrogen collisions.

In section III.A the assignment of the peaks of the hydrogen KED to collisions of H with Ar and Cl was based on the wave packet time evolution previously studied,[20] and on the energy position of the peaks (related to the amount of energy transferred collisionally). Analysis of the angular distributions of the H fragments associated with the different peaks of the KED provides an additional basis to confirm the previous assignment. To this purpose, the H fragment angular distributions associated with the main peak, the secondary peak, and the tail of the KED have been calculated, and they are shown in Figure 7 for the excitation energies studied.

As expected, the angular distribution associated with the main peak of the KED is the dominant one, and it is the main one responsible for the shape of the global distributions of Figure 6. The weight of this angular distribution increases with E, consistently with the increase of the weight of the main peak in the KED discussed in section III.A. This distribution consists essentially of a very intense peak around $\theta' = 50°$, and a long

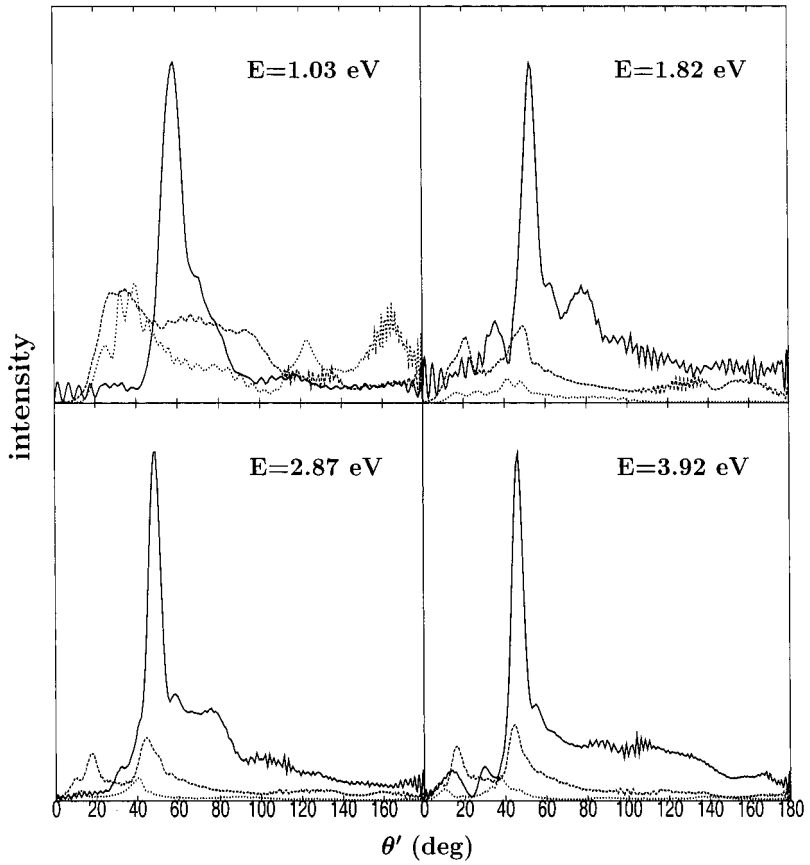

Figure 7. Angular distributions of the H fragment for the four excitation energies investigated. For each excitation energy the three angular distributions are associated with the main peak (solid line), the secondary peak (dashed line), and the tail (dotted line) of the corresponding KED.

tail extending toward larger angles. This angular pattern coincides with that of the most intense piece of wave packet produced after the first H/Ar collision, which confirms the previous assignment of the main peak of the KED. The corresponding H fragments are scattered in all possible directions, although mainly in the region $40° < \theta' < 80°$, following a nearly direct dissociation mechanism that involves a relatively weak collision with Ar. We note that the angular distributions associated with the main peak of the KED show some intensity at very small angles. This can be due to partial overlapping between the main and the secondary peaks in the KED. An additional and likely explanation is that components of the second wave packet piece (that appearing at small angles) also contribute, to a small extent, to the main peak of the KED.

The angular distributions associated with the secondary peak of the KED spread over the whole angular range, as well as the distributions corresponding to the main peak. Most of the angular intensity appears in the region $\theta' < 80°$, where the distributions typically show two peaks close to $\theta' = 20°$ and $\theta' = 50°$, respectively. For very low excitation energies, like $E =$ 1.03 eV, the angular distribution is less structured in the region $\theta' < 80°$. The angular distributions show that the previous assignment of the secondary peak of the KED to the wave packet piece appearing at small angles was too simplistic, and only partially correct. Indeed, components of the two main pieces of wave packet (not only that at small angles) contribute to this peak of the KED.

In addition to the structure of two peaks near $\theta' = 20°$ and $\theta' = 50°$, the angular distributions associated with the secondary peak display a diffuse structure of two bumps around $\theta' = 130°$ and $\theta' = 160°$. These two bumps correspond to hydrogen atoms that, after colliding once with Ar, bounce and undergo a relatively weak collision with Cl and then dissociate. Upon this weak H/Cl collision, interference between the TF states populated produces the structure of two bumps at large angles. The two angular peaks at $\theta' < 60°$ (resulting from the first H/Ar collision) would correspond to the region of higher kinetic energies of the secondary peak of the KED. Likewise, the two broader and less intense bumps at $\theta' > 120°$ (resulting from the first H/Cl collision) would be associated with the region of lower kinetic energies of the KED secondary peak. There appears that upon each collision of hydrogen with Ar or Cl, interference between the corresponding TF states populated develops a structure of (at least) two peaks in the angular distribution. One of the peaks appears at angles close to the forward direction of the collision ($\theta' = 20°$ and $\theta' = 160°$ for the H/Ar and H/Cl collisions, respectively), while the other peak occurs at more open angles ($\theta' = 50°$ and $\theta' = 130°$, respectively). The position of each peak would be related with the strength of the collision. Again, this behavior is very similar to that shown by the two main pieces of the wave packet[20] after the first H/Ar collision.

The angular distributions associated with the tails of the hydrogen KED present a similar behavior. In the case of $E =$ 1.03 eV two broad peaks are found for $\theta' > 100°$, and a structure of spikes is displayed for $\theta' < 60°$. For this excitation energy the tail of the KED shows two broad bumps with similar intensity (see inset of Figure 1). The bump at higher kinetic energies in the tail would be associated with the two angular peaks at $\theta' > 100°$. These peaks are produced by H atoms that dissociate after a relatively hard H/Cl collision (harder than the H/Cl collision producing the angular intensity at $\theta' > 120°$ associated with the secondary peak of the KED). Upon even harder H/Cl collisions, the H atoms bounce and undergo a

further collision with Ar, giving rise to the structure of angular peaks at $\theta' < 60°$, which is associated with the peak appearing at the lowest kinetic energies in the KED tail.

For the other three excitation energies the angular distributions show a structure of peaks at angles $\theta' < 60°$, but very little intensity at $\theta' > 100°$. The reason is that, for these excitation energies, most of the intensity corresponding to H fragments dissociated after the H/Cl collision appears in the angular distribution (at $\theta' > 100°$) associated with the secondary peak of the KED. This explains that one of the two peaks of the KED tails has a lower intensity (the peak at higher kinetic energies), and confirms that this peak is associated with H/Cl collisions. The angular intensity at $\theta' < 60°$, associated with the most intense bump of each KED tail, shows a structure of typically more than two peaks. The H fragments that produce this intensity have undergone three successive collisions (with Ar, Cl, and Ar, respectively) before dissociating. Interference between the TF states induced by the three successive collisions is probably the responsible of the richer angular structure at $\theta' < 60°$.

The angular distributions of Figure 7 indicate that a strong mixing of fragment states occurs, as a result of interference produced by the successive hydrogen collisions. Hydrogen fragments with relatively close kinetic energy can appear at very different final angles, and vice versa, H fragments with very different kinetic energies may be scattered at similar angles. These distributions may have interesting experimental implications. They show the angular regions where the H fragments with a given kinetic energy (within a certain range) are most likely to be detected. In general, at most of the angles the H fragments detected will sample a wide range of kinetic energies, although the region of very high kinetic energies will be dominant. However, due to the structure of the different angular distributions, there are angular regions where the intensity associated with the first weak H/Ar collisions is not the dominant one. These regions would be especially favorable to detect fragments more extensively cooled. As seen from Figure 7, this is the case of relatively small angles for all the excitation energies studied. For very low excitation energies (e.g., $E = 1.03$ eV) the intensity of cold fragments is also dominant at large angles. Therefore, by selecting the angular region where the hydrogen detector is placed, different regions of the H fragment KED can be probed in detail. The distributions of Figure 7 can provide a guide to these angular regions.

It should be noted, however, that the present angular distributions are calculated in the cluster body-fixed frame, with respect to the Ar−Cl axis of the cluster. As a consequence, the calculated distributions are not directly comparable with experimental distributions measured in the laboratory frame, and the structure found in the calculations could not be observed in the experimental distributions. A possibility to observe experimentally the angular structure could be to orient the Ar−HCl cluster by external fields.

IV. Concluding Remarks

The total fragmentation pathway of Ar−HCl upon ultraviolet photolysis, Ar−HCl + $h\nu \rightarrow$ H + Ar + Cl, is investigated by means of a wave packet calculation. Energy-resolved kinetic-energy release distributions of the H fragment are calculated for different excitation energies of Ar−HCl in the region of the absorption spectrum. In the range of kinetic energies studied (0.85 eV) the distributions display up to four peaks, which are associated with different collisional events of hydrogen with Ar and Cl. The most intense and narrowest peak, appearing at very high kinetic energies, is assigned to weak collisions where the hydrogen collides for the first time with Ar. Harder H/Ar collisions give rise to a secondary, broader peak at somewhat lower kinetic energies. As the kinetic energy decreases in the distribution, two additional broad bumps are found, assigned to further additional collisions of hydrogen with Cl and then with Ar again, respectively, before dissociating. Upon these multiple collisions the H fragment can be extensively cooled. The structure shown by the H kinetic-energy distributions is the signature of interference between broad overlapping resonance states in the excited surface of Ar−HCl where the hydrogen collides once or more with Ar and Cl. The structure associated with the main and secondary peaks of the distributions appears to be intense enough as to be experimentally observed. Manifestations of this interference are also found in the structure of the angular distributions of the recoiling H fragments. This structure reflects the number and the strength of the collisions undergone by the hydrogen before dissociation. As the number of hydrogen collisions increases, the interference between fragment states and the resulting angular structure becomes increasingly complicated.

Despite the fact that the structures manifested in the PF (refs 23 and 24) and the TF product distributions have a similar origin in interference between fragment states, there is an interesting difference between them. This difference is related to the specific fragment states that interfere. The interference manifestations in the distributions of the PF products[23,24] are produced mainly by interference between PF and TF states (and also between PF states themselves). Thus, manifestation of interference in the PF distributions involves the simultaneous population of both PF and TF states through the two fragmentation pathways of the cluster. In contrast, the main interference manifestations in the TF product distributions are produced by interference essentially only between TF states, which implies that such manifestations are rather independent of the simultaneous occurrence of the PF pathway. In this sense, depending on the kinetic-energy region where the H fragments are produced, one can distinguish two types of interference. In the region of very high kinetic energies, including the main peak of the H KED and higher kinetic energies, interference occurs between PF and TF states and between PF states themselves. The region of lower kinetic energies, including the secondary peak and the tail of the hydrogen KED, is governed by interference practically only between TF states.

The present analysis of the total fragmentation pathway of Ar−HCl complements the previous one of the partial fragmentation pathway,[24] and both together provide a global view of the Ar−HCl ultraviolet photolysis and its fragmentation mechanisms. The mechanism of total fragmentation of the cluster involving multiple hydrogen collisions and interference between the states populated by them appears to be quite general to other hydrogen-bonded clusters, as long as the hydrogen recoil is initially blocked by some obstacles (like Ar and Cl in Ar−HCl). Experimental investigation of the validity for Ar−HCl and other hydrogen-bonded clusters of the interpretation of the ultraviolet photolysis proposed here (and in ref 24) should be very interesting.

Acknowledgment. We akcnowledge helpful discussions with Dr. R. Prosmiti regarding the classical calculations. This work was supported by CICYT, Spain, Grant No. BCM-2001-2179, and by the EU network TMR Grant No. HPRN-CT-1999-00005.

References and Notes

(1) Jaques, C.; Valachovic, L.; Ionov, S.; Wen, Y.; Böhmer, E.; Segall, J.; Wittig, C. *J. Chem. Soc., Faraday Trans.* **1993**, *89*, 1419.

(2) Zhang, J.; Dulligan, M.; Segall, J.; Wen, Y.; Wittig, C. *J. Phys. Chem.* **1995**, *99*, 13680.

(3) Liu, K.; Kolessov, A.; Partin, J. W.; Bezel, I.; Wittig, C. *Chem. Phys. Lett.* **1999**, *299*, 374.

(4) Mackenzie, S. R.; Votava, O.; Fair, J. R.; Nesbitt, D. J. *J. Chem. Phys.* **1999**, *110*, 5149.

(5) Segall, J.; Wen, Y.; Singer, R.; Wittig, C.; García-Vela, A.; Gerber, R. B. *Chem. Phys. Lett.* **1993**, *207*, 504.

(6) Picconatto, C. A.; Ni, H.; Srivastava, A.; Valentini, J. J. *J. Chem. Phys.* **2001**, *114*, 7073.

(7) Plusquellic, D. F.; Votava, O.; Nesbitt, D. J. *J. Chem. Phys.* **1994**, *101*, 6356.

(8) Votava, O.; Plusquellic, D. F.; Myers, T. L.; Nesbitt, D. J. *J. Chem. Phys.* **2000**, *112*, 7449.

(9) Young, M. A. *J. Chem. Phys.* **1995**, *102*, 7925.

(10) Baumfalk, R.; Buck, U.; Frischkorn, C.; Nahler, N. H.; Hüwel, L. *J. Chem. Phys.* **1999**, *111*, 2595.

(11) Alimi, R.; Gerber, R. B. *Phys. Rev. Lett.* **1990**, *64*, 1453.

(12) McCoy, A. B.; Hurwitz, Y.; Gerber, R. B. *J. Phys. Chem.* **1993**, *97*, 12516.

(13) García-Vela, A.; Gerber, R. B.; Buck, U. *J. Phys. Chem.* **1994**, *98*, 3518.

(14) Christoffel, K. M.; Bowman, J. M. *J. Chem. Phys.* **1996**, *104*, 8348.

(15) García-Vela, A.; Gerber, R. B.; Valentini, J. J. *Chem. Phys. Lett.* **1991**, *186*, 223. *J. Chem. Phys.* **1992**, *97*, 3297.

(16) García-Vela, A.; Gerber, R. B.; Imre, D. G.; Valentini, J. J. *Phys. Rev. Lett.* **1993**, *71*, 931.

(17) García-Vela, A.; Gerber, R. B. *J. Chem. Phys.* **1993**, *98*, 427.

(18) Schröder, T.; Schinke, R.; Mandziuk, M.; Baciæ, Z. *J. Chem. Phys.* **1994**, *100*, 7239. Schröder, T.; Schinke, R.; Baciæ, Z. *Chem. Phys. Lett.* **1995**, *235*, 316.

(19) García-Vela, A.; Gerber, R. B. *J. Chem. Phys.* **1995**, *103*, 3463.

(20) García-Vela, A. *J. Chem. Phys.* **1998**, *108*, 5755.

(21) Narevicius, E.; Moiseyev, N. *Chem. Phys. Lett.* **1998**, *287*, 250. *Mol. Phys.* **1998**, *94*, 897.

(22) Juanes-Marcos, J. C.; García-Vela, A. *J. Chem. Phys.* **1999**, *111*, 2606.

(23) (a) Juanes-Marcos, J. C.; García-Vela, A. *J. Chem. Phys.* **2000**, *112*, 4983. (b) *J. Chem. Phys.* **2001**, *115*, 5692 (E).

(24) Juanes-Marcos, J. C.; García-Vela, A. *J. Phys. Chem. A* **2002**, *106*, 236.

(25) García-Vela, A. *J. Chem. Phys.* **2000**, *112*, 8302.

(26) The angular distribution of Figure 5b of ref 20 is plotted vs θ instead of θ', as the present angular distributions. However, as $R' \rightarrow \infty$ (or $r \rightarrow \infty$), the coordinates θ and θ' become very similar.